Structural Engineering and Mechanics, Vol. 35, No. 5 (2010) 593-616
DOI: http://dx.doi.org/10.12989/sem.2010.35.5.593

Seismic interaction of flexural ductility and shear capacity in reinforced concrete columns

Rachel Howser[1], A. Laskar[2] and *Y.L. Mo[1]

[1]*Department of Civil and Environmental Engineering, University of Houston, Houston, 77204-4003, USA*
[2]*WorleyParsons, Houston, 77094, USA*

(Received November 30, 2007, Accepted February 28, 2010)

Abstract. The seismic performance of reinforced concrete (RC) bridge columns is a significant issue because the interaction of flexural ductility and shear capacity of such columns with varied amounts of lateral reinforcement is not well established. Several relationships between flexural ductility and shear capacity have been proposed by various researchers in the past. In this paper, a parametric study on RC bridge columns is conducted using a nonlinear finite element program, "Simulation of Concrete Structures (SCS)", developed at the University of Houston. SCS has been previously used to predict the seismic behavior of such columns. The predicted results were compared with the test results obtained from experiments available in literature. Based on the results of the parametric study performed in this paper, a set of new relationships between flexural ductility and shear capacity of RC columns is proposed for seismic design.

Keywords: reinforced concrete; bridge columns; ductility; shear capacity.

1. Introduction

Shear failure in reinforced concrete (RC) bridge columns due to seismic loading has proven to be an issue in both experimental research and post-earthquake investigations. Columns are expected to be the primary elements of energy dissipation in bridges subjected to seismic loads. Failure of bridge columns often results in the collapse of bridge spans, as was the scenario for the majority of the bridges damaged in the past earthquakes. Thus the behavior of columns does play an essential role for earthquake resistant bridge design (Mo *et al.* 2003).

The seismic performance of RC bridge columns is of significant importance in places of high seismic activity. Since there is not yet a dependably accurate model that connects flexural ductility and shear capacity, RC bridge columns need to be studied further.

A number of models (ACI 2005, Caltrans 1995, Priestley *et al.* 1994, Sezen and Moehle 2004, Xiao and Martirossyan 1998) have been proposed to describe the interaction between flexural ductility and shear strength. However, these models have proven to either be gross over- or under-estimates, rendering them unusable in design. See Chapter 5 for a comparison of these models. When one investigates the relationship between shear capacity and flexural ductility, it is obvious

*Corresponding author, Professor, E-mail: yilungmo@egr.uh.edu

that the rate of change of shear capacity with ductility changes over the ductility domain. A major flaw in conventional shear design (ACI 2005) assumes that the shear capacity is not a function of ductility.

Previous models also assumed that the shear capacity provided by the shear reinforcement increases linearly as a function of the shear reinforcement. However, this assumption is incorrect. Increasing the stirrup ratio does increase the shear strength of the column; however, this phenomenon does not occur in a linear fashion according to the analytical study carried out by the University of Houston (UH) in this paper.

This paper reviews a number of previous shear capacity models, and proposes a new model. The newly proposed model is based on the results of an analytical study on RC columns performed using a nonlinear finite element program, "Simulation of Concrete Structures (SCS)", developed at UH. SCS has been validated by comparing its predictions with several sets of tests on shear walls and bridge columns under reversed cyclic loading and shake table excitation (Zhong 2005).

2. Previous shear strength models

Over the past few decades, many researchers have focused on shear strength models for RC. Five existing models were selected for examination in this work. They include the ACI 318 model (2005), the California Department of Transportation's (Caltrans) model (1995), a model proposed by the University of California, San Diego (UCSD) (Priestley *et al*. 1994), a proposed model from University of Southern California (USC) (Xiao and Martirossyan 1998), and a model proposed by the University of California, Berkeley (UCB) (Sezen and Moehle 2004). Each of the models is to be used for rectangular RC columns. The variables used in the equations can be found in Appendix II. Each of the models uses standard units unless stated otherwise.

2.1 ACI 318 model

The *ACI Building Code Requirements for Structural Concrete* (ACI 318-02 2005) provides a conservative model for shear strength. The model is to be used with English units.

$$V_n = V_c + V_s \tag{1}$$

$$V_c = 2\left(1 + \frac{P}{2000A_g}\right)\sqrt{f'_c}\, b_w d \tag{2}$$

$$V_s = \frac{A_v f_y d}{s} \tag{3}$$

2.2 Caltrans model

A similar model was proposed by Caltrans in their 1995 "Memo to Designers Change Letter 02". The key difference in this model compared to ACI's model is the recognition that ductility plays a role in the shear capacity of a member. Caltrans' nominal shear strength model's general equation is the same as that shown in Eq. (1). The rest of the model can be viewed in Eqs. (4) through (7).

$$V_c = F_1 F_2 \sqrt{f_c'} A_e \leq 4\sqrt{f_c'} A_e \tag{4}$$

$$0.3 \leq F_1 = \frac{\rho'' f_y}{150} + 3.67 - \mu \leq 3.0 \tag{5}$$

$$1.0 \leq F_2 = 0.0005\left(\frac{P}{A_g}\right) + 1 \leq 1.5 \tag{6}$$

$$V_s = \frac{A_v f_y h_c}{s} \tag{7}$$

2.3 UCSD model

Priestly *et al.* (1994) proposed a slightly different model. They emphasized the axial component of the shear strength model by defining it as a separate entity than the concrete component. They also factored flexural ductility into the model. Their model is shown in Eqs. (8) through (12).

$$V_n = V_c + V_p + V_s \tag{8}$$

$$V_c = k\sqrt{f_c'} A_e \tag{9}$$

$$k = 0.29 \quad \text{for} \quad \mu < 2.0 \tag{10a}$$

$$k = 0.29 - 0.095(\mu - 2) \quad \text{for} \quad 2.0 \leq \mu < 4.0 \tag{10b}$$

$$k = 0.1 \quad \text{for} \quad \mu \geq 4.0 \tag{10c}$$

$$V_p = \frac{D - c}{2a} P \tag{11}$$

$$V_s = \frac{A_v f_y D'}{s} \cot(30^\circ) \tag{12}$$

2.4 USC model

The University of Southern California (Xiao and Martirossyan 1998) expanded on UCSD's model to provide a model that would more accurately predict the effects of using high strength concrete. The most significant change was the presentation of a bilinear model for ductilities between two and six. Their model is shown below. The model uses the same general equation shown in Eq. (8) and the same equation for the concrete contribution to shear shown in Eq. (9).

$$k = 0.29 \quad \text{for} \quad \mu < 2.0 \tag{13a}$$

$$k = 0.29 - 0.12(\mu - 2) \quad \text{for} \quad 2.0 \leq \mu < 4.0 \tag{13b}$$

$$k = 0.05 - 0.025(\mu - 4) \quad \text{for} \quad 4.0 \leq \mu \leq 6.0 \tag{13c}$$

$$k = 0 \quad \text{for} \quad \mu > 6.0 \tag{13d}$$

$$V_p = \frac{D-c}{2D(M/VD)}P \tag{14}$$

$$V_s = \frac{A_v f_y (d-c)}{s}\cot(\theta) \tag{15}$$

2.5 UCB model

UCB (Sezen and Moehle 2004) proposed yet a different model. This model was similar to UCSD and Caltrans' models in that flexural ductility was a primary contributor to the model. The model is shown in Eqs. (16) through (18). The same general equation was used as described in Eq. (1). This model is to be used with English units.

$$V_c = k\left(\frac{6\sqrt{f_c'}}{a/d}\sqrt{1+\frac{P}{6\sqrt{f_c'}A_g}}\right)0.8A_g \tag{16}$$

$$k = 1.00 \quad \text{for} \quad \mu < 2.0 \tag{17a}$$

$$k = 1.00 - 0.075(\mu - 2) \quad \text{for} \quad 2.0 \le \mu < 6.0 \tag{17b}$$

$$k = 0.70 \quad \text{for} \quad \mu \ge 6.0 \tag{17c}$$

$$V_s = k\frac{A_v f_y d}{s} \tag{18}$$

3. "Simulation of Concrete Structures" (SCS) and parametric studies

Over the past two decades, UH has performed a significant amount of research for the purpose of predicting shear behavior of RC structures. This research resulted in a series of constitutive models of which the Cyclic Softened Membrane Model (CSMM) (Mansour and Hsu 2005a, b), a rational model that incorporates the Poisson effect and cyclic constitutive laws of concrete and mild steel bars, is the most recent. This model has been shown to accurately predict the cyclic shear behavior of RC membrane elements. CSMM was implemented into OpenSees, a finite element framework developed at UCB (Fenves 2005), and a nonlinear finite element computer program, "Simulation of Concrete Structures" (SCS) was developed (Zhong 2005). The program is capable of predicting the nonlinear behavior of RC and prestressed concrete structures subjected to various types of loading, including monotonic and reverse cyclic loading as well as shake table excitation (Laskar 2009). SCS is unique in that it is the only program to implement CSMM and is capable of predicting post-peak behavior of concrete structures. In addition to CSMM, SCS also includes beam-column elements available in the standard version of OpenSEES. This allows for modeling of the flexural behavior of concrete structures. SCS also considers an increased concrete core compressive strength

caused by the stirrup confinement as proposed by Scott *et al.* (1982).

SCS's accuracy was validated by testing three full-scale hollow rectangular RC bridge columns at the National Center for Research on Earthquake Engineering (NCREE) in Taiwan (Mo *et al.* 2006). The test set up for the columns is shown in Fig. 1. The dimensions and properties of each of the columns are shown in Table 1 and Fig. 2. Each specimen was tested under displacement control, following a predetermined displacement history defined in terms of drift percentage. This is shown in Fig. 3. The flexure-critical columns were tested cyclically up to a drift percentage of 7.5%. The

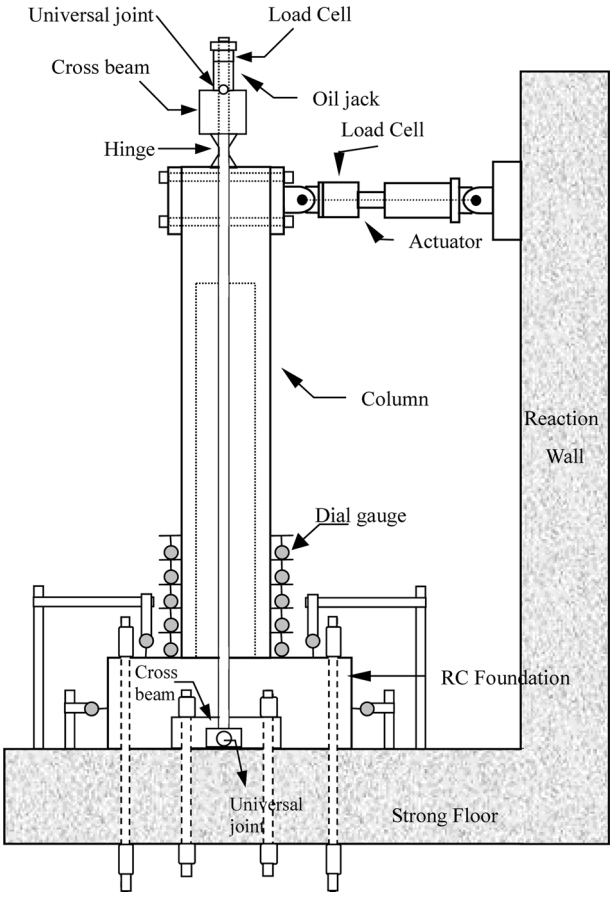

Fig. 1 Test set-up

Table 1 Dimensions and properties of bridge columns

ID No.	f_c' (MPa)	P (kN)	$\frac{P}{f_c' A_g}$	L (mm)	Longitudinal Reinforcement			Transverse Reinforcement		
					Dia. (mm)	f_y (MPa)	f_{su} (MPa)	Dia. (mm)	f_y (MPa)	Spacing (mm)
PS1	34.0	4000	0.082	6500	22	460.0	647.0	13	343.0	80
PI1	34.0	4000	0.082	4500	22	460.0	647.0	10	510.0	120
PI2	32.0	3600	0.078	3500	22	418.2	626.5	10	420.0	200

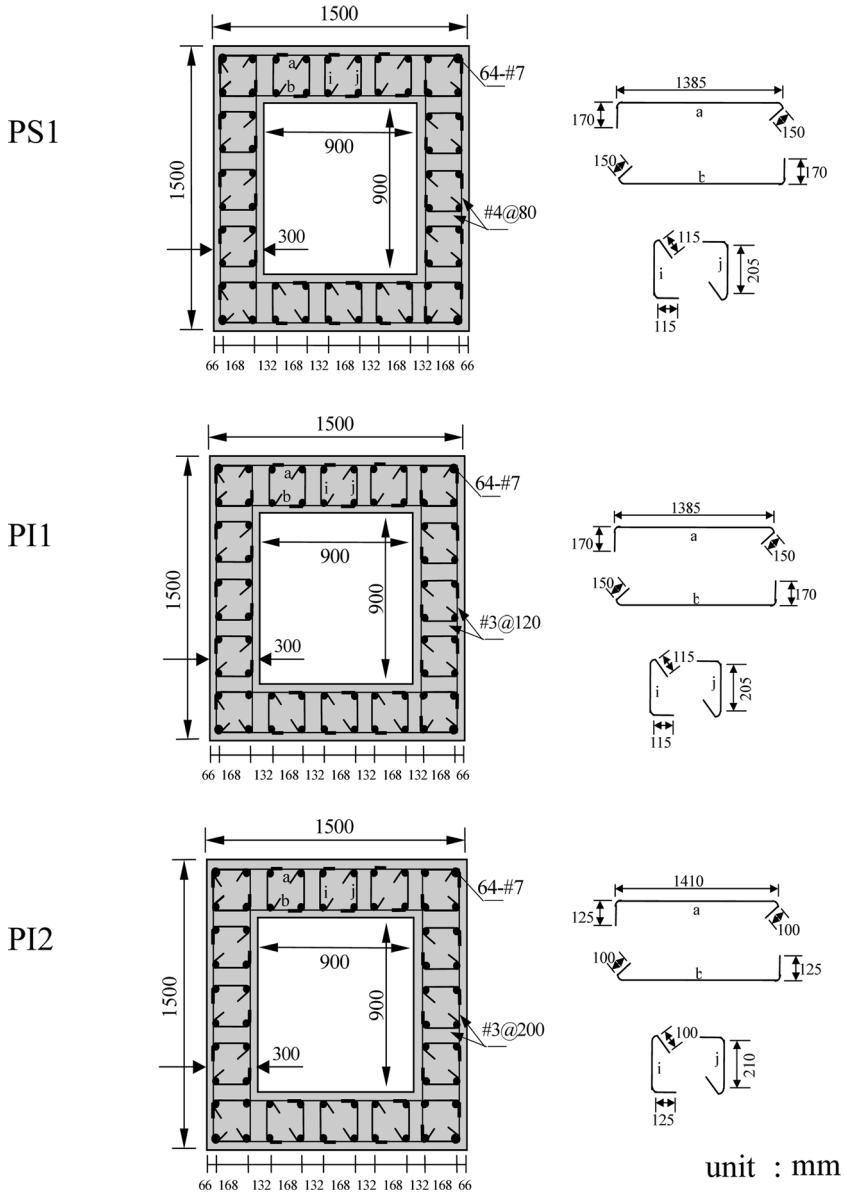

Fig. 2 Dimensions and reinforcement of the cross-section (Mo *et al.* 2006)

shear-critical columns were tested cyclically up to a drift percentage of 3.5%. SCS did an excellent job in predicting the results of the tests. Experimental and predicted load-deformation plots for the three specimens are shown in Figs. 4, 5, and 6. It is noted that the failure mode of Specimen PI2 is shear.

Since SCS can accurately predict seismic behavior, it can be implemented for the use of amassing a considerable amount of data in order to come up with a more accurate model that predicts the relationship between flexural ductility and shear strength of RC columns. Since Specimen PI2 was shear governed, it was chosen as a template for future specimens. Specimen PI2's physical

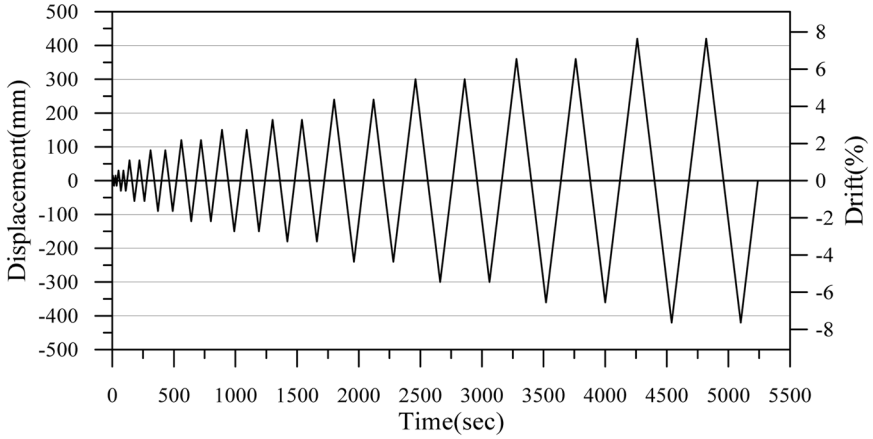

(a) Specimen PS1-C , PI1-C

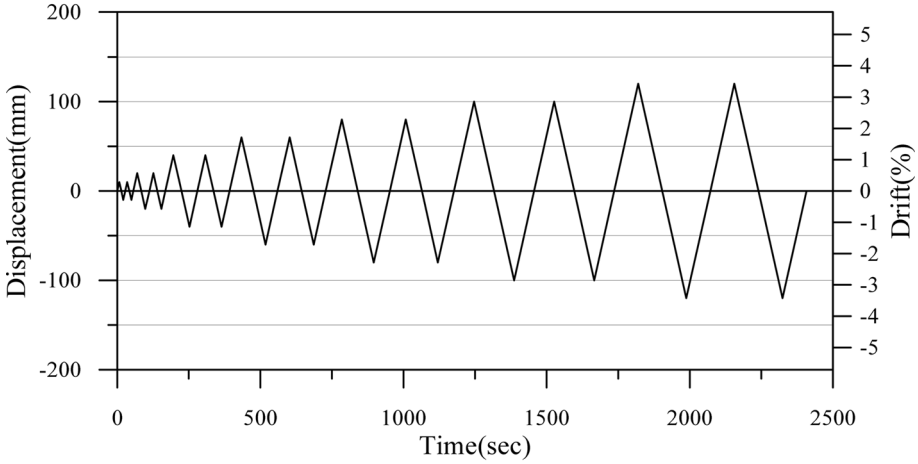

(b) Specimen PI2-C

Fig. 3 Loading history

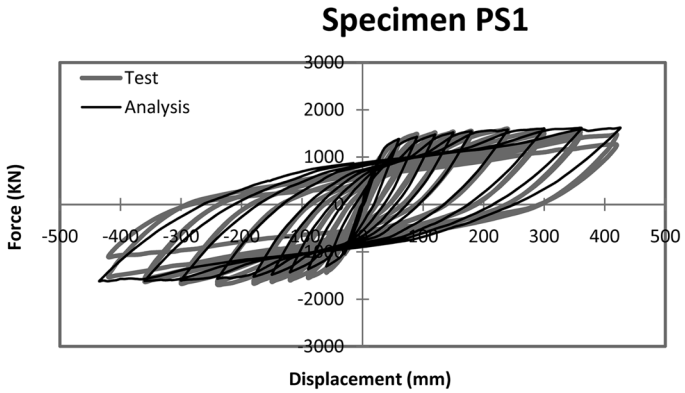

Fig. 4 Predicted vs. experimental force-displacement curves of specimen PS1

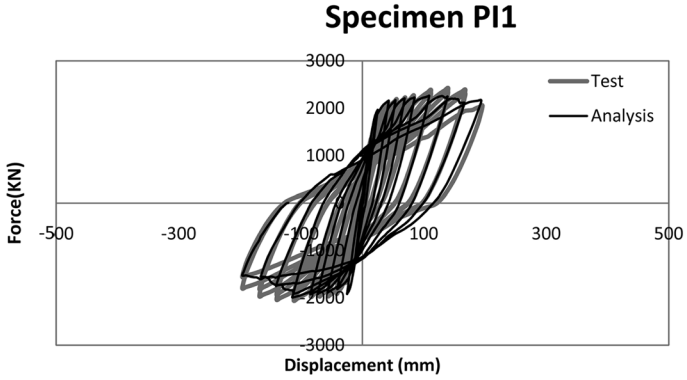

Fig. 5 Predicted vs. experimental force-displacement curves of specimen PI1

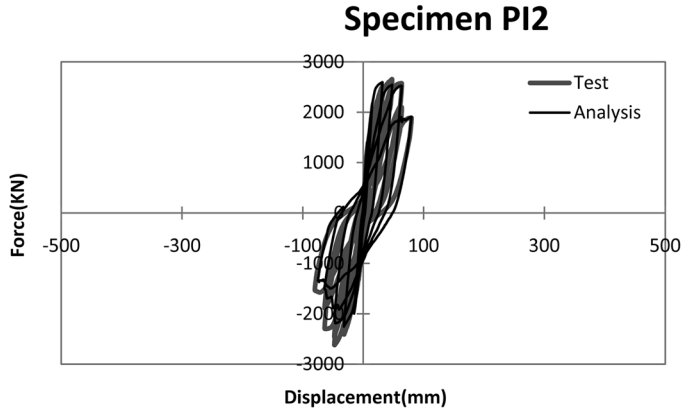

Fig. 6 Predicted vs. experimental force-displacement curves of specimen PI2

characteristics were varied for the purpose of effectively building and testing other columns in the developed program. This method is preferred over actually testing columns because of the expense and time involved in testing a real column. The modeled columns provide a quick, free, alternative that produces nearly identical results as the real tests. In this manner, one can perform many experiments quickly and can analyze many sets of results instead of the few made practical by the high cost of testing actual columns.

Initially, two parameters were varied while the rest coincided with Specimen PI2. These two variables were the stirrup ratio and longitudinal steel ratio. Next the compressive strength was increased and the process was repeated. Each theoretical specimen's parameters are shown in Table 2. Each of these specimens was in turn analyzed using SCS and a curve was developed that enveloped the extreme points of the hystersis loops for each specimen. Fig. 7 shows the envelope curve for one of the specimens analyzed using SCS. While the aspect ratio was not varied for the parametric studies, it was determined that the proposed model works for a variety of aspect ratios. This is shown in Chapter 7.

Table 2 Specimen properties

Specimen	Ag (mm^2)	Av (mm^2)	a (mm)	bw (mm)	c (mm)	D (mm)	D' (mm)	d (mm)	f_c' (MPa)	f_y (MPa)	h_c (mm)	P (N)	s (mm)	p_t (%)	p_l (%)	V (kN)	Ductility
PI2-14-024-0170	1440000	576	3000	600	241	1500	1380	1350	14	414	690	3600	200	1.70	0.24	1643	2.90
PI2-21-024-0170	1440000	576	3000	600	209	1500	1380	1350	21	414	690	3600	200	1.70	0.24	1840	3.12
PI2-28-024-0170	1440000	576	3000	600	188	1500	1380	1350	28	414	690	3600	200	1.70	0.24	1985	3.29
PI2-32-024-0050	1440000	576	3000	600	178	1500	1380	1350	32	414	690	3491	200	0.50	0.24	1636	4.55
PI2-32-024-0100	1440000	576	3000	600	178	1500	1380	1350	32	414	690	3491	200	1.00	0.24	1819	4.95
PI2-32-024-0170	1440000	576	3000	600	177	1500	1380	1350	32	414	690	3600	200	1.70	0.24	2040	3.52
PI2-32-024-0170	1440000	576	3000	600	178	1500	1380	1350	32	414	690	3600	200	1.70	0.24	2040	3.52
PI2-32-024-0200	1440000	576	3000	600	178	1500	1380	1350	32	414	690	3491	200	2.00	0.24	2120	3.31
PI2-32-024-0300	1440000	576	3000	600	178	1500	1380	1350	32	414	690	3491	200	3.00	0.24	2330	2.78
PI2-32-024-0400	1440000	576	3000	600	178	1500	1380	1350	32	414	690	3491	200	4.00	0.24	2493	2.61
PI2-32-024-0500	1440000	576	3000	600	178	1500	1380	1350	32	414	690	3491	200	5.00	0.24	2616	2.49
PI2-32-024-0600	1440000	576	3000	600	178	1500	1380	1350	32	414	690	3502	200	6.00	0.24	2691	2.49
PI2-32-024-0700	1440000	576	3000	600	178	1500	1380	1350	32	414	690	3502	200	7.00	0.24	2743	2.55
PI2-32-024-0800	1440000	576	3000	600	178	1500	1380	1350	32	414	690	3502	200	8.00	0.24	2766	2.64
PI2-32-050-0050	1440000	1200	3000	600	178	1500	1380	1350	32	414	690	3502	200	0.50	0.50	1796	4.25
PI2-32-050-0100	1440000	1200	3000	600	178	1500	1380	1350	32	414	690	3491	200	1.00	0.50	1974	4.73
PI2-32-050-0170	1440000	1200	3000	600	178	1500	1380	1350	32	414	690	3502	200	1.70	0.50	2192	3.94
PI2-32-050-0200	1440000	1200	3000	600	178	1500	1380	1350	32	414	690	3491	200	2.00	0.50	2272	3.70
PI2-32-050-0300	1440000	1200	3000	600	178	1500	1380	1350	32	414	690	3502	200	3.00	0.50	2564	3.03
PI2-32-050-0400	1440000	1200	3000	600	178	1500	1380	1350	32	414	690	3502	200	4.00	0.50	2767	2.73
PI2-32-050-0500	1440000	1200	3000	600	178	1500	1380	1350	32	414	690	3502	200	5.00	0.50	2974	2.48
PI2-32-050-0600	1440000	1200	3000	600	178	1500	1380	1350	32	414	690	3502	200	6.00	0.50	3142	2.30
PI2-32-050-0700	1440000	1200	3000	600	178	1500	1380	1350	32	414	690	3502	200	7.00	0.50	3258	2.19
PI2-32-050-0800	1440000	1200	3000	600	178	1500	1380	1350	32	414	690	3512	200	8.00	0.50	3341	2.14
PI2-32-050-0900	1440000	1200	3000	600	178	1500	1380	1350	32	414	690	3512	200	9.00	0.50	3399	2.16
PI2-32-075-0050	1440000	1800	3000	600	178	1500	1380	1350	32	414	690	3512	200	0.50	0.75	1896	3.53
PI2-32-075-0100	1440000	1800	3000	600	178	1500	1380	1350	32	414	690	3512	200	1.00	0.75	2066	4.05
PI2-32-075-0170	1440000	1800	3000	600	178	1500	1380	1350	32	414	690	3512	200	1.70	0.75	2280	4.21

Table 2 Continued

Specimen	Ag (mm^2)	Av (mm^2)	a (mm)	bw (mm)	c (mm)	D (mm)	D' (mm)	d (mm)	f_c' (MPa)	f_y (MPa)	h_c (mm)	P (N)	s (mm)	p_t (%)	p_l (%)	V (kN)	Ductility
PI2-32-075-0200	1440000	1800	3000	600	178	1500	1380	1350	32	414	690	3502	200	2.00	0.75	2374	3.86
PI2-32-075-0300	1440000	1800	3000	600	178	1500	1380	1350	32	414	690	3512	200	3.00	0.75	2660	3.27
PI2-32-075-0400	1440000	1800	3000	600	178	1500	1380	1350	32	414	690	3512	200	4.00	0.75	2913	2.83
PI2-32-075-0500	1440000	1800	3000	600	178	1500	1380	1350	32	414	690	3512	200	5.00	0.75	3134	2.64
PI2-32-075-0600	1440000	1800	3000	600	178	1500	1380	1350	32	414	690	3512	200	6.00	0.75	3330	2.43
PI2-32-075-0700	1440000	1800	3000	600	178	1500	1380	1350	32	414	690	3512	200	7.00	0.75	3498	2.24
PI2-32-075-0800	1440000	1800	3000	600	178	1500	1380	1350	32	414	690	3512	200	8.00	0.75	3626	2.10
PI2-32-075-0900	1440000	1800	3000	600	178	1500	1380	1350	32	414	690	3522	200	9.00	0.75	3719	1.95
PI2-32-100-0050	1440000	2400	3000	600	178	1500	1380	1350	32	414	690	3522	200	0.50	1.00	1947	3.42
PI2-32-100-0100	1440000	2400	3000	600	178	1500	1380	1350	32	414	690	3522	200	1.00	1.00	2120	3.73
PI2-32-100-0170	1440000	2400	3000	600	178	1500	1380	1350	32	414	690	3533	200	1.70	1.00	2340	3.92
PI2-32-100-0200	1440000	2400	3000	600	178	1500	1380	1350	32	414	690	3522	200	2.00	1.00	2432	3.91
PI2-32-100-0300	1440000	2400	3000	600	178	1500	1380	1350	32	414	690	3522	200	3.00	1.00	2726	3.32
PI2-32-100-0400	1440000	2400	3000	600	178	1500	1380	1350	32	414	690	3522	200	4.00	1.00	2995	2.89
PI2-32-100-0500	1440000	2400	3000	600	178	1500	1380	1350	32	414	690	3522	200	5.00	1.00	3211	2.66
PI2-32-100-0600	1440000	2400	3000	600	178	1500	1380	1350	32	414	690	3522	200	6.00	1.00	3446	2.46
PI2-32-100-0700	1440000	2400	3000	600	178	1500	1380	1350	32	414	690	3522	200	7.00	1.00	3637	2.27
PI2-32-100-0800	1440000	2400	3000	600	178	1500	1380	1350	32	414	690	3522	200	8.00	1.00	3808	2.02
PI2-32-100-0900	1440000	2400	3000	600	178	1500	1380	1350	32	414	690	3533	200	9.00	1.00	3932	1.92
PI2-32-125-0100	1440000	3000	3000	600	178	1500	1380	1350	32	414	690	3533	200	1.00	1.25	2140	3.68
PI2-32-125-0170	1440000	3000	3000	600	178	1500	1380	1350	32	414	690	3543	200	1.70	1.25	2358	3.87
PI2-32-125-0200	1440000	3000	3000	600	178	1500	1380	1350	32	414	690	3533	200	2.00	1.25	2455	3.81
PI2-32-125-0300	1440000	3000	3000	600	178	1500	1380	1350	32	414	690	3533	200	3.00	1.25	2762	3.42
PI2-32-125-0400	1440000	3000	3000	600	178	1500	1380	1350	32	414	690	3533	200	4.00	1.25	3049	2.88
PI2-32-125-0500	1440000	3000	3000	600	178	1500	1380	1350	32	414	690	3533	200	5.00	1.25	3268	2.65
PI2-32-125-0600	1440000	3000	3000	600	178	1500	1380	1350	32	414	690	3533	200	6.00	1.25	3504	2.41
PI2-32-125-0700	1440000	3000	3000	600	178	1500	1380	1350	32	414	690	3533	200	7.00	1.25	3712	2.22
PI2-32-125-0800	1440000	3000	3000	600	178	1500	1380	1350	32	414	690	3533	200	8.00	1.25	3895	2.06

Table 2 Continued

Specimen	Ag (mm^2)	Av (mm^2)	a (mm)	bw (mm)	c (mm)	D (mm)	D' (mm)	d (mm)	f_c' (MPa)	f_y (MPa)	h_c (mm)	P (N)	s (mm)	p_t (%)	p_l (%)	V (kN)	Ductility
PI2-32-125-0900	1440000	3000	3000	600	178	1500	1380	1350	32	414	690	3543	200	9.00	1.25	4051	1.93
PI2-32-150-0100	1440000	3600	3000	600	178	1500	1380	1350	32	414	690	3543	200	1.00	1.50	2155	3.81
PI2-32-150-0170	1440000	3600	3000	600	178	1500	1380	1350	32	414	690	3553	200	1.70	1.50	2369	3.92
PI2-32-150-0200	1440000	3600	3000	600	178	1500	1380	1350	32	414	690	3543	200	2.00	1.50	2465	3.89
PI2-32-150-0300	1440000	3600	3000	600	178	1500	1380	1350	32	414	690	3543	200	3.00	1.50	2773	3.42
PI2-32-150-0400	1440000	3600	3000	600	178	1500	1380	1350	32	414	690	3543	200	4.00	1.50	3075	2.98
PI2-32-150-0500	1440000	3600	3000	600	178	1500	1380	1350	32	414	690	3543	200	5.00	1.50	3303	2.73
PI2-32-150-0600	1440000	3600	3000	600	178	1500	1380	1350	32	414	690	3543	200	6.00	1.50	3545	2.50
PI2-32-150-0700	1440000	3600	3000	600	178	1500	1380	1350	32	414	690	3543	200	7.00	1.50	3771	2.31
PI2-32-150-0800	1440000	3600	3000	600	178	1500	1380	1350	32	414	690	3543	200	8.00	1.50	3963	2.16
PI2-32-150-0900	1440000	3600	3000	600	178	1500	1380	1350	32	414	690	3553	200	9.00	1.50	4130	1.98
PI2-32-175-0100	1440000	4200	3000	600	178	1500	1380	1350	32	414	690	3553	200	1.00	1.75	2170	3.69
PI2-32-175-0170	1440000	4200	3000	600	178	1500	1380	1350	32	414	690	3564	200	1.70	1.75	2375	4.11
PI2-32-175-0200	1440000	4200	3000	600	178	1500	1380	1350	32	414	690	3553	200	2.00	1.75	2471	4.06
PI2-32-175-0300	1440000	4200	3000	600	178	1500	1380	1350	32	414	690	3553	200	3.00	1.75	2775	3.50
PI2-32-175-0400	1440000	4200	3000	600	178	1500	1380	1350	32	414	690	3553	200	4.00	1.75	3078	3.04
PI2-32-175-0500	1440000	4200	3000	600	178	1500	1380	1350	32	414	690	3553	200	5.00	1.75	3337	2.75
PI2-32-175-0600	1440000	4200	3000	600	178	1500	1380	1350	32	414	690	3553	200	6.00	1.75	3581	2.51
PI2-32-175-0700	1440000	4200	3000	600	178	1500	1380	1350	32	414	690	3553	200	7.00	1.75	3815	2.35
PI2-32-175-0800	1440000	4200	3000	600	178	1500	1380	1350	32	414	690	3553	200	8.00	1.75	3999	2.16
PI2-32-175-0900	1440000	4200	3000	600	178	1500	1380	1350	32	414	690	3553	200	9.00	1.75	4182	2.02
PI2-32-175-1000	1440000	4200	3000	600	178	1500	1380	1350	32	414	690	3564	200	10.00	1.75	4342	1.90
PI2-32-200-0100	1440000	4800	3000	600	178	1500	1380	1350	32	414	690	3564	200	1.00	2.00	2182	3.74
PI2-32-200-0170	1440000	4800	3000	600	178	1500	1380	1350	32	414	690	3491	200	1.70	2.00	2379	4.14
PI2-32-200-0200	1440000	4800	3000	600	178	1500	1380	1350	32	414	690	3564	200	2.00	2.00	2476	4.08
PI2-32-200-0300	1440000	4800	3000	600	178	1500	1380	1350	32	414	690	3564	200	3.00	2.00	2781	3.57
PI2-32-200-0400	1440000	4800	3000	600	178	1500	1380	1350	32	414	690	3564	200	4.00	2.00	3086	3.10
PI2-32-200-0500	1440000	4800	3000	600	178	1500	1380	1350	32	414	690	3564	200	5.00	2.00	3363	2.82

Table 2 Continued

Specimen	Ag (mm^2)	Av (mm^2)	a (mm)	bw (mm)	c (mm)	D (mm)	D' (mm)	d (mm)	f_c' (MPa)	f_y (MPa)	h_c (mm)	P (N)	s (mm)	p_t (%)	p_l (%)	V (kN)	Ductility
PI2-32-200-0600	1440000	4800	3000	600	178	1500	1380	1350	32	414	690	3564	200	6.00	2.00	3609	2.54
PI2-32-200-0700	1440000	4800	3000	600	178	1500	1380	1350	32	414	690	3564	200	7.00	2.00	3845	2.34
PI2-32-200-0800	1440000	4800	3000	600	178	1500	1380	1350	32	414	690	3564	200	8.00	2.00	4038	2.22
PI2-32-200-0900	1440000	4800	3000	600	178	1500	1380	1350	32	414	690	3564	200	9.00	2.00	4225	2.05
PI2-32-200-1000	1440000	4800	3000	600	178	1500	1380	1350	32	414	690	3600	200	10.00	2.00	4403	1.92
PI2-34-024-0170	1440000	576	3000	600	172	1500	1380	1350	34	414	690	3600	200	1.70	0.24	2058	3.70
PI2-41-024-0170	1440000	576	3000	600	160	1500	1380	1350	41	414	690	3600	200	1.70	0.24	2109	4.11
PI2-48-024-0170	1440000	576	3000	600	151	1500	1380	1350	48	414	690	3600	200	1.70	0.24	2159	4.39
PI2-55-024-0025	1440000	576	3000	600	61	1500	1380	1350	55	414	690	3600	200	0.25	0.24	1533	2.91
PI2-55-024-0050	1440000	576	3000	600	84	1500	1380	1350	55	414	690	3600	200	0.50	0.24	1478	1.99
PI2-55-024-0100	1440000	576	3000	600	114	1500	1380	1350	55	414	690	3600	200	1.00	0.24	1958	5.32
PI2-55-024-0170	1440000	576	3000	600	143	1500	1380	1350	55	414	690	3600	200	1.70	0.24	2199	4.45
PI2-55-024-0200	1440000	576	3000	600	152	1500	1380	1350	55	414	690	3600	200	2.00	0.24	2307	4.11
PI2-55-024-0300	1440000	576	3000	600	179	1500	1380	1350	55	414	690	3600	200	3.00	0.24	2593	3.59
PI2-55-024-0400	1440000	576	3000	600	200	1500	1380	1350	55	414	690	3600	200	4.00	0.24	2805	3.06
PI2-55-024-0500	1440000	576	3000	600	216	1500	1380	1350	55	414	690	3600	200	5.00	0.24	2968	2.78
PI2-55-024-0600	1440000	576	3000	600	231	1500	1380	1350	55	414	690	3600	200	6.00	0.24	3107	2.62
PI2-55-024-0700	1440000	576	3000	600	243	1500	1380	1350	55	414	690	3600	200	7.00	0.24	3436	2.21
PI2-55-024-0800	1440000	576	3000	600	254	1500	1380	1350	55	414	690	3600	200	8.00	0.24	3282	2.87
PI2-55-050-0050	1440000	1200	3000	600	84	1500	1380	1350	55	414	690	3600	200	0.50	0.50	1908	6.61
PI2-55-050-0100	1440000	1200	3000	600	114	1500	1380	1350	55	414	690	3600	200	1.00	0.50	2111	6.60
PI2-55-050-0170	1440000	1200	3000	600	143	1500	1380	1350	55	414	690	3600	200	1.70	0.50	2380	5.96
PI2-55-050-0200	1440000	1200	3000	600	152	1500	1380	1350	55	414	690	3600	200	2.00	0.50	2471	5.67
PI2-55-050-0300	1440000	1200	3000	600	179	1500	1380	1350	55	414	690	3600	200	3.00	0.50	2787	4.19
PI2-55-050-0400	1440000	1200	3000	600	200	1500	1380	1350	55	414	690	3600	200	4.00	0.50	3084	3.33
PI2-55-050-0500	1440000	1200	3000	600	216	1500	1380	1350	55	414	690	3600	200	5.00	0.50	3296	2.95
PI2-55-050-0600	1440000	1200	3000	600	231	1500	1380	1350	55	414	690	3600	200	6.00	0.50	3499	2.76
PI2-55-050-0700	1440000	1200	3000	600	243	1500	1380	1350	55	414	690	3600	200	7.00	0.50	3672	2.62

Table 2 Continued

Specimen	Ag (mm^2)	Av (mm^2)	a (mm)	bw (mm)	c (mm)	D (mm)	D' (mm)	d (mm)	f_c' (MPa)	f_y (MPa)	h_c (mm)	P (N)	s (mm)	p_t (%)	p_l (%)	V (kN)	Ductility
PI2-55-050-0800	1440000	1200	3000	600	254	1500	1380	1350	55	414	690	3600	200	8.00	0.50	3836	2.47
PI2-55-050-0900	1440000	1200	3000	600	263	1500	1380	1350	55	414	690	3600	200	9.00	0.50	3949	2.41
PI2-55-050-1000	1440000	1200	3000	600	272	1500	1380	1350	55	414	690	3600	200	10.00	0.50	4036	2.38
PI2-55-050-1100	1440000	1200	3000	600	280	1500	1380	1350	55	414	690	3600	200	11.00	0.50	4094	2.39
PI2-55-075-0050	1440000	1800	3000	600	84	1500	1380	1350	55	414	690	3600	200	0.50	0.75	2038	4.91
PI2-55-075-0100	1440000	1800	3000	600	114	1500	1380	1350	55	414	690	3600	200	1.00	0.75	2218	5.41
PI2-55-075-0300	1440000	1800	3000	600	179	1500	1380	1350	55	414	690	3600	200	3.00	0.75	2908	4.11
PI2-55-075-0400	1440000	1800	3000	600	200	1500	1380	1350	55	414	690	3600	200	4.00	0.75	3202	3.52
PI2-55-075-0500	1440000	1800	3000	600	216	1500	1380	1350	55	414	690	3600	200	5.00	0.75	3476	3.13
PI2-55-075-0600	1440000	1800	3000	600	231	1500	1380	1350	55	414	690	3600	200	6.00	0.75	3678	2.91
PI2-55-075-0700	1440000	1800	3000	600	243	1500	1380	1350	55	414	690	3600	200	7.00	0.75	3883	2.68
PI2-55-075-0800	1440000	1800	3000	600	254	1500	1380	1350	55	414	690	3600	200	8.00	0.75	4090	2.57
PI2-55-075-0900	1440000	1800	3000	600	263	1500	1380	1350	55	414	690	3600	200	9.00	0.75	4263	2.36
PI2-55-075-1000	1440000	1800	3000	600	272	1500	1380	1350	55	414	690	3600	200	10.00	0.75	4405	2.25
PI2-55-075-1100	1440000	1800	3000	600	280	1500	1380	1350	55	414	690	3600	200	11.00	0.75	4508	2.18
PI2-55-075-1200	1440000	1800	3000	600	287	1500	1380	1350	55	414	690	3600	200	12.00	0.75	4593	2.15
PI2-55-075-200	1440000	1800	3000	600	152	1500	1380	1350	55	414	690	3600	200	2.00	0.75	2594	5.06
PI2-55-100-0050	1440000	2400	3000	600	84	1500	1380	1350	55	414	690	3600	200	0.50	1.00	2099	4.19
PI2-55-100-0100	1440000	2400	3000	600	114	1500	1380	1350	55	414	690	3600	200	1.00	1.00	2288	4.47
PI2-55-100-0200	1440000	2400	3000	600	152	1500	1380	1350	55	414	690	3600	200	2.00	1.00	2675	4.73
PI2-55-100-0300	1440000	2400	3000	600	179	1500	1380	1350	55	414	690	3600	200	3.00	1.00	2989	4.29
PI2-55-100-0400	1440000	2400	3000	600	200	1500	1380	1350	55	414	690	3600	200	4.00	1.00	3276	3.87
PI2-55-100-0500	1440000	2400	3000	600	216	1500	1380	1350	55	414	690	3600	200	5.00	1.00	3560	3.33
PI2-55-100-0600	1440000	2400	3000	600	231	1500	1380	1350	55	414	690	3600	200	6.00	1.00	3819	3.04
PI2-55-100-0700	1440000	2400	3000	600	243	1500	1380	1350	55	414	690	3600	200	7.00	1.00	4026	2.76
PI2-55-100-0800	1440000	2400	3000	600	254	1500	1380	1350	55	414	690	3600	200	8.00	1.00	4257	2.63
PI2-55-100-0900	1440000	2400	3000	600	263	1500	1380	1350	55	414	690	3600	200	9.00	1.00	4450	2.48
PI2-55-100-1000	1440000	2400	3000	600	272	1500	1380	1350	55	414	690	3600	200	10.00	1.00	4620	2.24

Table 2 Continued

Specimen	Ag (mm^2)	Av (mm^2)	a (mm)	bw (mm)	c (mm)	D (mm)	D' (mm)	d (mm)	f_c' (MPa)	f_y (MPa)	h_c (mm)	P (N)	s (mm)	p_t (%)	p_l (%)	V (kN)	Ductility
PI2-55-100-1100	1440000	2400	3000	600	280	1500	1380	1350	55	414	690	3600	200	11.00	1.00	4762	2.12
PI2-55-100-1200	1440000	2400	3000	600	287	1500	1380	1350	55	414	690	3600	200	12.00	1.00	4871	2.05
PI2-55-125-0050	1440000	3000	3000	600	84	1500	1380	1350	55	414	690	3600	200	0.50	1.25	2158	3.63
PI2-55-125-0100	1440000	3000	3000	600	114	1500	1380	1350	55	414	690	3600	200	1.00	1.25	2347	3.91
PI2-55-125-0200	1440000	3000	3000	600	152	1500	1380	1350	55	414	690	3600	200	2.00	1.25	2748	4.37
PI2-55-125-0300	1440000	3000	3000	600	179	1500	1380	1350	55	414	690	3600	200	3.00	1.25	3064	4.11
PI2-55-125-0400	1440000	3000	3000	600	200	1500	1380	1350	55	414	690	3600	200	4.00	1.25	3353	3.69
PI2-55-125-0500	1440000	3000	3000	600	216	1500	1380	1350	55	414	690	3600	200	5.00	1.25	3632	3.27
PI2-55-125-0600	1440000	3000	3000	600	231	1500	1380	1350	55	414	690	3600	200	6.00	1.25	3901	3.07
PI2-55-125-0700	1440000	3000	3000	600	243	1500	1380	1350	55	414	690	3600	200	7.00	1.25	4111	2.85
PI2-55-125-0800	1440000	3000	3000	600	254	1500	1380	1350	55	414	690	3600	200	8.00	1.25	4360	2.56
PI2-55-125-0900	1440000	3000	3000	600	263	1500	1380	1350	55	414	690	3600	200	9.00	1.25	4592	2.37
PI2-55-125-1000	1440000	3000	3000	600	272	1500	1380	1350	55	414	690	3600	200	10.00	1.25	4778	2.32
PI2-55-125-1100	1440000	3000	3000	600	280	1500	1380	1350	55	414	690	3600	200	11.00	1.25	4951	2.11
PI2-55-125-1200	1440000	3000	3000	600	287	1500	1380	1350	55	414	690	3600	200	12.00	1.25	5086	2.02
PI2-55-150-0050	1440000	3600	3000	600	84	1500	1380	1350	55	414	690	3600	200	0.50	1.50	2208	3.81
PI2-55-150-0100	1440000	3600	3000	600	114	1500	1380	1350	55	414	690	3600	200	1.00	1.50	2379	4.19
PI2-55-150-0200	1440000	3600	3000	600	152	1500	1380	1350	55	414	690	3600	200	2.00	1.50	2786	4.03
PI2-55-150-0300	1440000	3600	3000	600	179	1500	1380	1350	55	414	690	3600	200	3.00	1.50	3103	3.99
PI2-55-150-0400	1440000	3600	3000	600	200	1500	1380	1350	55	414	690	3600	200	4.00	1.50	3402	3.67
PI2-55-150-0500	1440000	3600	3000	600	216	1500	1380	1350	55	414	690	3600	200	5.00	1.50	3684	3.32
PI2-55-150-0600	1440000	3600	3000	600	231	1500	1380	1350	55	414	690	3600	200	6.00	1.50	3955	3.03
PI2-55-150-0700	1440000	3600	3000	600	243	1500	1380	1350	55	414	690	3600	200	7.00	1.50	4175	2.84
PI2-55-150-0800	1440000	3600	3000	600	254	1500	1380	1350	55	414	690	3600	200	8.00	1.50	4417	2.66
PI2-55-150-0900	1440000	3600	3000	600	263	1500	1380	1350	55	414	690	3600	200	9.00	1.50	4658	2.41
PI2-55-150-1000	1440000	3600	3000	600	272	1500	1380	1350	55	414	690	3600	200	10.00	1.50	4866	2.26
PI2-55-150-1100	1440000	3600	3000	600	280	1500	1380	1350	55	414	690	3600	200	11.00	1.50	5049	2.13
PI2-55-150-1200	1440000	3600	3000	600	287	1500	1380	1350	55	414	690	3600	200	12.00	1.50	5220	2.02

Table 2 Continued

Specimen	Ag (mm^2)	Av (mm^2)	a (mm)	bw (mm)	c (mm)	D (mm)	D' (mm)	d (mm)	f_c' (MPa)	f_y (MPa)	h_c (mm)	P (N)	s (mm)	p_t (%)	p_l (%)	V (kN)	Ductility
PI2-55-175-0050	1440000	4200	3000	600	84	1500	1380	1350	55	414	690	3600	200	0.50	1.75	2249	3.48
PI2-55-175-0100	1440000	4200	3000	600	114	1500	1380	1350	55	414	690	3600	200	1.00	1.75	2399	4.06
PI2-55-175-0200	1440000	4200	3000	600	152	1500	1380	1350	55	414	690	3600	200	2.00	1.75	2812	3.93
PI2-55-175-0300	1440000	4200	3000	600	179	1500	1380	1350	55	414	690	3600	200	3.00	1.75	3126	3.96
PI2-55-175-0400	1440000	4200	3000	600	200	1500	1380	1350	55	414	690	3600	200	4.00	1.75	3425	3.76
PI2-55-175-0500	1440000	4200	3000	600	216	1500	1380	1350	55	414	690	3600	200	5.00	1.75	3720	3.35
PI2-55-175-0600	1440000	4200	3000	600	231	1500	1380	1350	55	414	690	3600	200	6.00	1.75	4001	3.05
PI2-55-175-0700	1440000	4200	3000	600	243	1500	1380	1350	55	414	690	3600	200	7.00	1.75	4221	2.88
PI2-55-175-0800	1440000	4200	3000	600	254	1500	1380	1350	55	414	690	3600	200	8.00	1.75	4462	2.74
PI2-55-175-0900	1440000	4200	3000	600	263	1500	1380	1350	55	414	690	3600	200	9.00	1.75	4705	2.53
PI2-55-175-1000	1440000	4200	3000	600	272	1500	1380	1350	55	414	690	3600	200	10.00	1.75	4926	2.31
PI2-55-175-1100	1440000	4200	3000	600	280	1500	1380	1350	55	414	690	3600	200	11.00	1.75	5118	2.18
PI2-55-175-1200	1440000	4200	3000	600	287	1500	1380	1350	55	414	690	3600	200	12.00	1.75	5295	2.06
PI2-55-200-0050	1440000	4800	3000	600	84	1500	1380	1350	55	414	690	3600	200	0.50	2.00	2323	2.98
PI2-55-200-0100	1440000	4800	3000	600	114	1500	1380	1350	55	414	690	3600	200	1.00	2.00	2412	3.94
PI2-55-200-0200	1440000	4800	3000	600	152	1500	1380	1350	55	414	690	3600	200	2.00	2.00	2826	4.29
PI2-55-200-0300	1440000	4800	3000	600	179	1500	1380	1350	55	414	690	3600	200	3.00	2.00	3141	3.96
PI2-55-200-0400	1440000	4800	3000	600	200	1500	1380	1350	55	414	690	3600	200	4.00	2.00	3432	3.77
PI2-55-200-0500	1440000	4800	3000	600	216	1500	1380	1350	55	414	690	3600	200	5.00	2.00	3730	3.43
PI2-55-200-0600	1440000	4800	3000	600	231	1500	1380	1350	55	414	690	3600	200	6.00	2.00	4023	3.11
PI2-55-200-0700	1440000	4800	3000	600	243	1500	1380	1350	55	414	690	3600	200	7.00	2.00	4259	2.92
PI2-55-200-0800	1440000	4800	3000	600	254	1500	1380	1350	55	414	690	3600	200	8.00	2.00	4500	2.70
PI2-55-200-0900	1440000	4800	3000	600	263	1500	1380	1350	55	414	690	3600	200	9.00	2.00	4744	2.54
PI2-55-200-1000	1440000	4800	3000	600	272	1500	1380	1350	55	414	690	3600	200	10.00	2.00	4974	2.39
PI2-55-200-1100	1440000	4800	3000	600	280	1500	1380	1350	55	414	690	3600	200	11.00	2.00	5169	2.22
PI2-55-200-1200	1440000	4800	3000	600	287	1500	1380	1350	55	414	690	3600	200	12.00	2.00	5352	2.11

4. Determination of flexural ductility and shear capacity

After the envelope curves were developed for each of the analyzed specimens, the flexural ductility and shear capacity of the specimens were estimated using a method described by Zahn *et al*. (1990). The displacement at the first yield point was estimated as the displacement that would be reached at the flexural strength if the stiffness of the member was that of the cracked member in the elastic range. This stiffness is obtained by determining the deflection that corresponds with 75 percent of the flexural strength on the envelope curve. The line passing through this point and the origin is then obtained and extended to determine the deflection associated with the flexural strength. The displacement corresponding to shear failure, or ultimate displacement, was assumed to occur along the enveloping curve at 80 percent of the flexural strength along the descending part of the curve. The flexural ductility was then taken to be the ratio between the ultimate and first yield point displacements. Fig. 7 shows a graphical interpretation of this method. This process was followed for each specimen. The flexural ductility and shear strength are shown in Table 2. Plots comparing shear strength and flexural ductility are shown in Figs. 8 and 9 for normal (32 MPa) and high (55 MPa) strength concrete respectively.

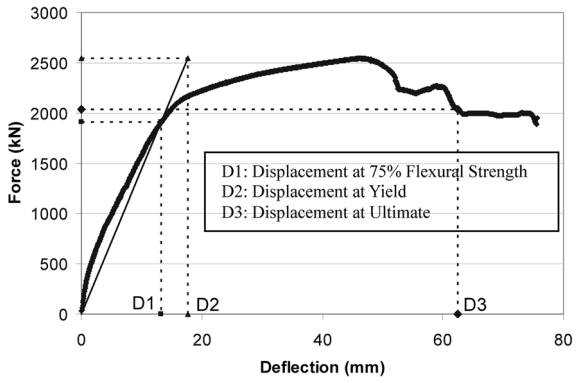

Fig. 7 Determination of the deflection at first yield

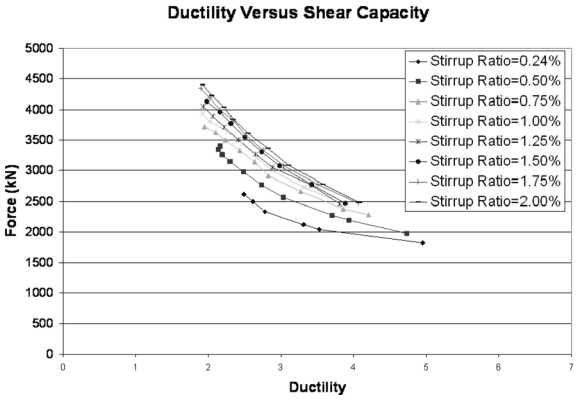

Fig. 8 Ductility versus shear strength for normal strength specimens

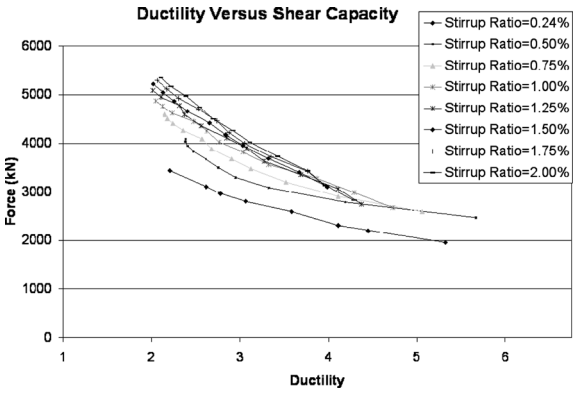

Fig. 9 Ductility versus shear strength for high strength specimens

5. Comparison of results obtained from SCS with current models

A comparative study was performed for each of the current models by dividing the ultimate shear strengths of all the specimens predicted using SCS by the shear strengths predicted using each model. The shear strength ratios were plotted against flexural ductility, stirrup ratio, and longitudinal steel ratio as they were the only varying parameters in this study. A visual perception of the comparative prediction of shear strengths for each of the models with respect to the results obtained using SCS can be obtained via Figs. 10 through 14.

From Fig. 10, it can be seen that average shear strengths predicted by ACI's model are close to that predicted from SCS. However, the variation between the results predicted from the two is quite large. Predictions obtained from Caltrans' model were often found to be slightly lower than the SCS predictions as shown in Fig. 11. The variation between the two predictions is also large. The predictions from the Caltrans model are much lower than the SCS predictions for low stirrup and longitudinal steel ratios. As seen in Fig. 12, predictions from UCSD's model are higher than that of SCS. However, the two predictions showed similar trends. Fig. 13 shows that USC's model also makes higher predictions when compared to SCS with variations similar to the UCSD predictions. The predictions from both UCSD and UCB's models were considerably higher than the SCS predictions as the stirrup ratio increased. A similar trend was shown for UCB's model in Fig. 14.

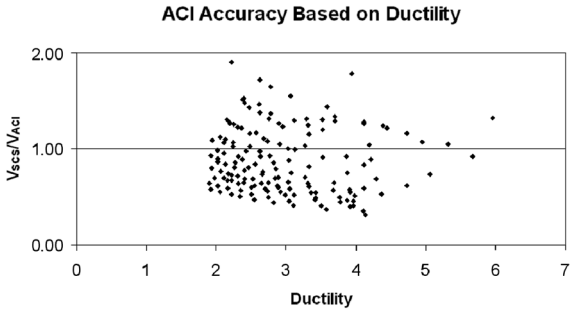

Fig. 10 Visual depiction of the accuracy of ACI's model

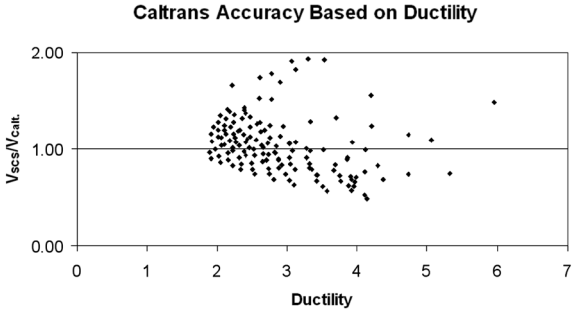

Fig. 11 Visual depiction of the accuracy of Caltrans' model

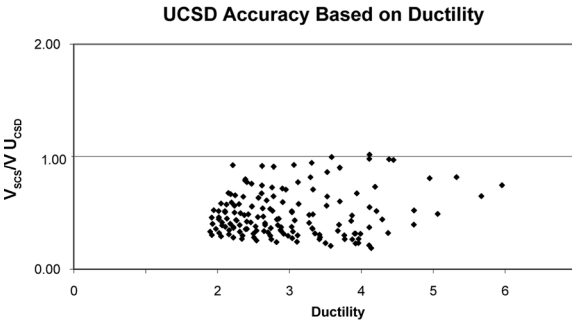

Fig. 12 Visual depiction of the accuracy of UCSD's model

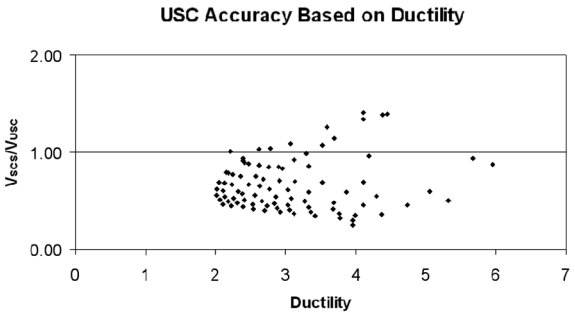

Fig. 13 Visual depiction of the accuracy of USC's model

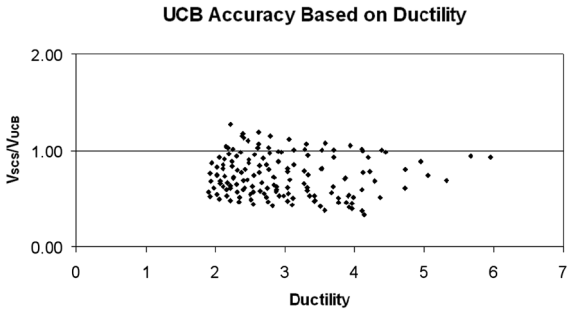

Fig. 14 Visual depiction of the accuracy of UCB's model

6. Proposed model

The model proposed as part of this work is applicable to any strength RC columns. The model is based on UCSD's model because results predicted from the UCSD's model were in agreement with results obtained using SCS in that the spread of the data was relatively small. The general equation for nominal shear strength of RC columns was the same as that used for UCSD's model as seen in Eq. (8) and consists of contributions due to concrete, axial load, and steel as derived through data regression.

6.1 Concrete contribution to shear

Following UCSD's model the concrete contribution to the shear capacity of RC structures is shown in Eq. (9). Many factors were considered to propose a relationship for the concrete contribution of the shear capacity, V_c, as it relates to the flexural ductility of RC structures. All previous models agree that V_c of RC structures remained unaffected by ductility of the structure up to a ductility of two. This does not seem affected by aspect ratio since UCB studied columns with an aspect ratio ranging from 2.22 to 3.87 (Sezen and Moehle 2004), USC studied columns with an aspect ratio of 2.00 (Xiao and Martirossyan 1998), and UCSD studied aspect ratios varying from 0.90 to 2.70 (Priestly *et al*. 1994). UH studied tests completed by Wight and Sozen (1975) with an aspect ratio of 3.45, Mo and Nien (2002) with aspect ratios ranging from 3.41 to 4.09 and Xiao and Martirossyan (1998) with an aspect ratio of 5.24. These tests also seemed to maintain a V_c unaffected by ductility up to a ductility of two despite the varied aspect ratios. Additionally, for aspect ratios less than two, columns are generally entirely shear governed. The flexural ductility of such columns is very small. This goal of this study was to find the relationship between shear capacity and flexural ductility, so such columns were not considered. This lower limit of ductility corresponding with two seems consistent with the data gathered.

For a ductility greater than two, V_c is observed to decrease with an increase in ductility. However, beyond an upper limit of ductility, V_c is again observed to remain constant with increasing ductility. Current models do not concur with this upper limit of ductility beyond which V_c remains constant. The data collected seems to indicate that this upper limit of ductility, q, varies and is directly proportional to the stirrup ratio for specimens having stirrup ratios up to a certain limit. For specimens having higher stirrup ratios, the ductility q becomes equal to the ductility r at which the decrease rate of shear capacity changes. The shear capacities of these specimens remain constant at

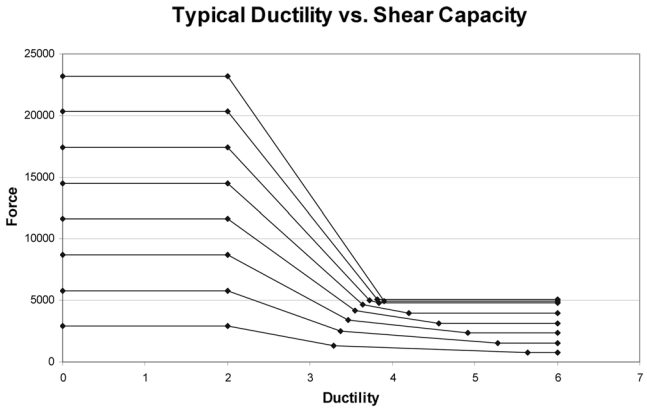

Fig. 15 Visual representation of idealized shape of ductility vs. force functions in proposed model

ductilities higher than *r*. See Fig. 15 for a visual representation of the relationship between shear force and flexural ductility. The relationship between the upper limit of ductility and the transverse steel ratio can be modeled as shown in Eqs. (20a) and (20b). The variable *r* is defined in Eqs. (20c).

$$q = -144\rho_t + 0.03f_c' + 4.3 \quad \text{for} \quad q \geq r \tag{20a}$$

$$q = r \quad \text{for} \quad q < r \tag{20b}$$

The next aspect explored was the relationship between V_c and flexural ductility between the upper and lower limits of ductility. It was apparent that the relationships depicted in Figs. 8 and 9 seem to follow a curve or two straight lines rather than a single straight line for low stirrup ratios. It was decided to propose a bilinear model similar to USC's model. The ductility at which the slope of the line changes varies rather than being constant; however, it was observed to correspond with the ductility of specimens having a longitudinal steel ratio of approximately four percent. With the data gathered from this research, the ductility at a longitudinal steel ratio of four percent varies with the tranverse steel ratio and concrete compressive strength and can be estimated as shown in Eq. (20c).

$$r = 35\rho_t - 0.011f_c' + 3.8 \tag{20c}$$

It was discovered the slopes used in USC's bilinear model were very close to the slopes observed in the data gathered. USC's model was therefore modified to fit the analytical results obtained using SCS as shown in Eq. (21).

$$k = 0.29 \quad \text{for} \quad \mu < 2.0 \tag{21a}$$

$$k = 0.29 - 0.12(\mu - 2) \quad \text{for} \quad 2.0 \leq \mu < r \tag{21b}$$

$$k = 0.53 - 0.095r - 0.025\mu \quad \text{for} \quad r \leq \mu \leq q \tag{21c}$$

$$k = 0.53 - 0.095r - 0.025q \quad \text{for} \quad \mu > q \tag{21d}$$

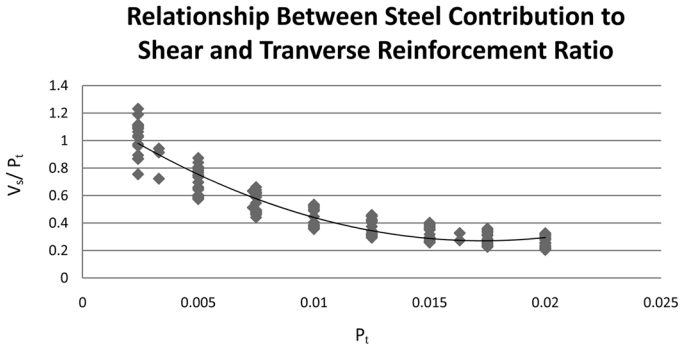

Fig. 16 Relationship between steel contribution to shear and tranverse reinforcement ratio

6.2 Shear contribution due to axial load

The shear resistance of RC structures due to the axial loads acting on them was found to depend on the same parameters as that in UCSD's model and is given in Eq. (22).

$$V_p = \frac{D-c}{2a}P \tag{22}$$

6.3 Steel contribution to shear

After implementing the new influence factor for flexural ductility into the UCSD's model for V_c, it was observed that the shear strengths estimated from the new model were significantly higher. Further study revealed that V_s proposed by UCSD's model were higher than the total shear capacities of the specimens studied herein. Hence a factor was needed to reduce the steel contribution to shear proposed by UCSD. This factor was chosen based on a regression analysis. Fig. 16 shows the relationship between the steel contribution of shear and the tranverse steel ratio. A new V_s is proposed in this study by modifying the V_s proposed by UCSD shown in Eq. (23).

$$V_s = (3200\rho_t^3 - 110\rho_t^2 + 1.2\rho_t)b_w f_{yh}(d-c)\cot(\theta) \tag{23}$$

7. Determination of the accuracy of the proposed models

Using the previously established method, the accuracy of the proposed model can be viewed in Fig. 17. As one can see in the figure, the ratio of the ultimate shear strengths of the specimens predicted using SCS to the shear strengths predicted using the new model is close to one and the scatter is greatly reduced. To further test the accuracy of the new model, it was used to calculate the shear capacities of a series of columns tested experimentally. Properties of the tested columns are shown in Tables 3 through 5 and the accuracy of the models can be seen in Figs. 18 through 23. The scatter of the strength ratios obtained from the new model was much smaller and fell closer to

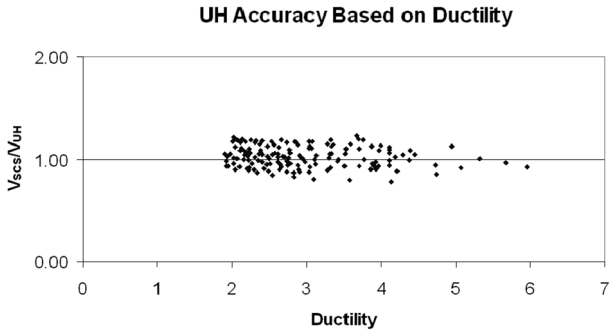

Fig. 17 Visual depiction of the accuracy of the proposed model

Table 3 Specimen properties for Wight and Sozen's tests (1975)

Specimen	ρ_l (%)	ρ_t (%)	$f'(c)$ (MPa)	Ductility	Ag (mm^2)	D (mm)	c (mm)	a (mm)	P (kN)	bw (mm)	fy (MPa)	d (mm)	a/d	V (kN)
40.033a	2.40	0.33	34.7	4.2	46452	305	52	876	189	152	344	254	3.45	77
40.033	2.40	0.33	33.6	3.6	46452	305	52	876	178	152	344	254	3.45	78
0.033	2.40	0.33	32.0	3.7	46452	305	52	876	0	152	344	254	3.45	65

Table 4 Specimen properties for Mo and Nien's tests (2002)

Specimen	ρ_l (%)	ρ_t (%)	$f'(c)$ (MPa)	Ductility	Ag (mm^2)	D (mm)	c (mm)	a (mm)	P (kN)	bw (mm)	fy (MPa)	d (mm)	a/d	V (kN)
HI-2-a	1.87	0.74	61.1	3.9	182400	500	48	1800	1500	240	363	440	4.09	350
HI-1-b	1.87	0.74	50.5	4.4	182400	500	52	1500	1000	240	363	440	3.41	364
HI-0-b	1.87	0.74	49.7	4.7	182400	500	52	1500	500	240	363	440	3.41	302

Table 5 Specimen properties for Xiao and Martirossyan's tests (1998)

Specimen	ρ_l (%)	ρ_t (%)	$f'(c)$ (MPa)	Ductil-ity	Ag (mm^2)	D (mm)	c (mm)	a (mm)	P (kN)	bw (mm)	fy (MPa)	d (mm)	a/d	V (kN)
HC4-8L16-T6-0.1P	2.48	1.63	86.0	6.0	64516	254	19	1016	534	254	510	194	5.24	218
HC4-8L16-T6-0.2P	2.48	1.63	86.0	4.0	64516	254	19	1016	1068	254	510	194	5.24	259

one than any of the other models. The scatter observed in the proposed model was expected since real columns are not built perfectly. However, the close results imply that the new proposed model works well for rectangular specimens of various concrete compressive strengths, sizes, configurations, and steel ratios. Additionally, the tested columns represented a variety of aspect ratios varying from 3.41 to 5.24, implying that the model is sufficiently accurate for different aspect ratios.

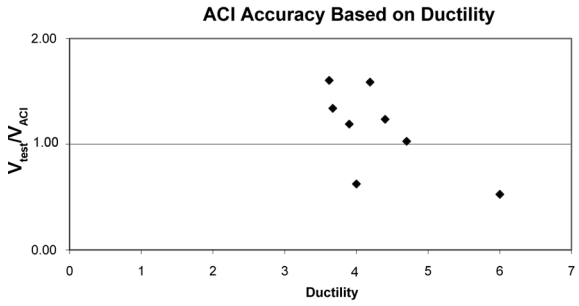

Fig. 18 Visual depiction of the accuracy of the ACI model using tested specimens

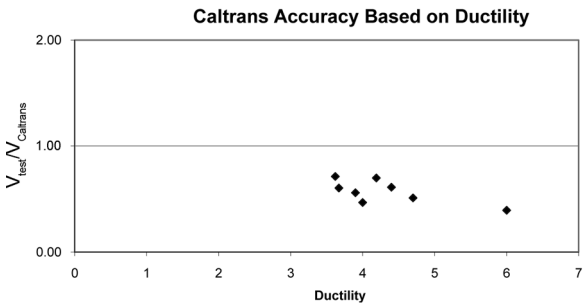

Fig. 19 Visual depiction of the accuracy of the Caltrans model using tested specimens

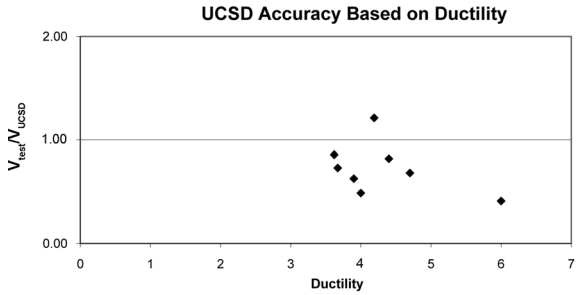

Fig. 20 Visual depiction of the accuracy of the UCSD model using tested specimens

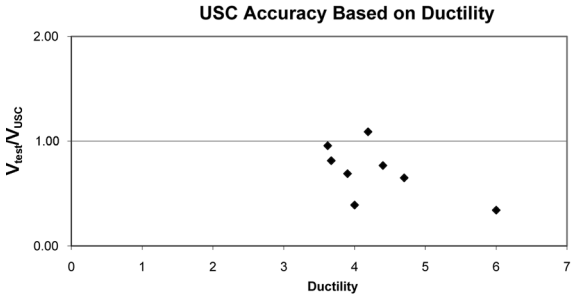

Fig. 21 Visual depiction of the accuracy of the USC model using tested specimens

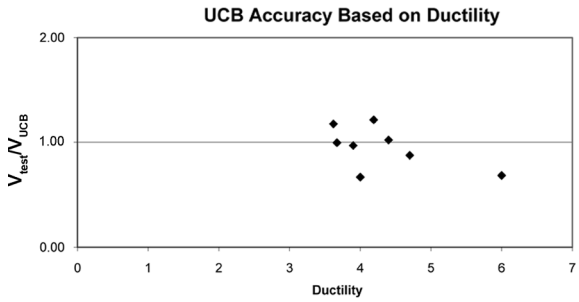

Fig. 22 Visual depiction of the accuracy of the UCB model using tested specimens

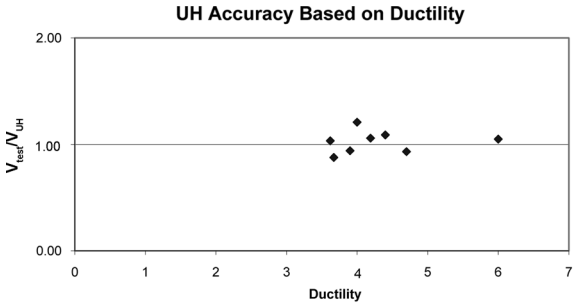

Fig. 23 Visual depiction of the accuracy of the proposed model using tested specimens

8. Conclusions

A finite element analysis program, "Simulation of Concrete Structures" (SCS) was developed at the University of Houston that is capable of accurately predicting the monotonic and cyclic behavior of reinforced concrete structures. Using this program, a series of rectangular columns was simulated and a model was proposed to predict the relationship between flexural ductility and shear capacity. Parameters varied in the study include the longitudinal and tranverse steel ratios in addition to the

concrete compressive strength. Other parameters such as a possible size affect or the aspect ratio were not considered in the parametric study; however, the model was in good agreement with experimental results of varied sizes and aspect ratios. This model was compared against six other models and was validated through comparison with a series of experimental tests. Through this work, the following conclusions can be drawn:

1. SCS is capable of accurately predicting the nonlinear behavior of RC columns subjected to cyclic loading.
2. There are several models available that predict the relationship between flexural ductility and shear strength; however, the accuracy of these models is doubtful due to either over- or under-estimations. Hence, they cannot be used in practice.
3. The proposed models can accurately predict the relationship between flexural ductility and shear strength in rectangular columns.

Acknowledgements

The research study described herein was sponsored by the National Science Foundation under the Award No. EEC-0649163. The opinions expressed in this study are those of the authors and do not necessarily reflect the views of the sponsor.

References

ACI Committee 318 (2005), "Building code requirements for structural concrete", *Farmington Hills, Mich*., 147-159.

Caltrans (1995), "Memo to Designers Change Letter 02", California Department of Transportation, Sacramento, Calif., March.

Fenves, G.L. (2005), "Annual workshop on open system for earthquake engineering simulation", Pacific Earthquake Engineering Research Center, UC Berkeley, http://opensees.berkeley.edu/.

Laskar, A. (2009), "Shear behavior and design of prestressed concrete members", Ph.D. Dissertation, Department of Civil and Environmental Engineering, University of Houston, Houston.

Mansour, M. and Hsu, T.T.C. (2005a), "Behavior of RC elements under cyclic shear: Part I-Experiments", *J. Struct. Eng.-ASCE*, **131**(1), 44-53.

Mansour, M. and Hsu, T.T.C. (2005b), "Behavior of RC elements under cyclic shear: Part 2-Theoretical model," *J. Struct. Eng.-ASCE*, **131**(1), 54-65.

Mo, Y.L. and Nien, I.C. (2002), "Seismic performance of hollow high-strength concrete bridge columns", *J. Bridge Eng.-ASCE*, **7**(6), 338-349.

Mo, Y.L., Wong, D.C. and Maekawa, K. (2003), "Seismic performance of hollow columns", *ACI Struct. J.*, **100**(3), 337-349.

Mo, Y.L., Yeh, Y.K., Zhong, J. and Hsu, T.T.C. (2006), "Seismic behavior of shear-critical hollow bridge columns", ASCE Structures Congress, St. Louis, MO, May.

Priestley, M.J.N., Verma, R. and Xiao, Y. (1994), "Seismic shear strength of RC columns", *J. Struct. Eng.-ASCE*, **120**(8), 2310-2329.

Scott, B.D., Park, R. and Priestley, M.J.N. (1982), "Stress-strain behavior of concrete confined by overlapping hoops at low and high strain rates", *ACI J.*, **79**(2), 13-27.

Sezen, H. and Moehle, J.P. (2004), "Shear strength model for lightly RC columns", *J. Struct. Eng.-ASCE*, **130**(11), 1692-1703.

Wight, J.K. and Sozen, M.A. (1975), "Strength decay of RC columns under shear reversals", *J. Struct. Div-*

ASCE, **101**(5), 1053-1065.
Xiao, Y. and Martirossyan, A. (1998), "Seismic performance of high-strength concrete columns", *J. Struct. Eng.-ASCE*, **124**(3), 241-251.
Zahn, F.A., Park, R. and Priestley, M.J.N. (1990), "Flexural strength and ductility of circular hollow RC columns without confinement on inside face", *ACI Struct. J.*, **87**(2), 156-166.
Zhong, J.X. (2005), "Model-based simulation of RC plane stress structures", PhD Dissertation, Dept. of Civil and Environmental Engineering, University of Houston, Houston, TX.

Notations

A_e : 80% of the cross-sectional area
A_g : the gross area of section
A_v : the area of shear reinforcement within a the distance of s
a : the ratio of the moment to the shear at the critical section
b_w : web width
c : the depth of the compression zone
D : the overall section depth
D' : the distance between the centers of the peripheral hoop or spiral
d : the distance from the extreme compression fiber to the centriod of the longitudinal tension reinforcement
F_1 : Factor 1, Caltrans Model
F_2 : Factor 2, Caltrans Model
f_c' : specified compressive strength of the concrete
f_y : the specified yield strength of nonprestressed reinforcement
h_c : the distance from the centerline of the hoop to the center of the cross section
k : factor for influence of flexural ductility
M/VD : the shear aspect ratio
P : the factored axial load normal to the cross section occurring simultaneously with the factored shear force at the section
q : upper limit of flexural ductility beyond which the shear capacity remains constant
r : flexural ductility at which the rate of decrease of shear capacity with flexural ductility changes
s : spacing of shear reinforcement measured in a direction parallel to longitudinal reinforcement
V_n : the nominal shear strength
V_c : the nominal shear strength provided by the concrete
V_p : the nominal shear strength provided by the axial load
V_s : the nominal shear strength provided by the shear reinforcement
μ : the displacement ductility
ρ_t : the ratio of the transverse reinforcement volume to gross column volume, A_v/sb_w
ρ_l : the ratio of the longitudinal steel volume to gross column volume
θ : angle of principal shear crack to column axis